Surfaces and Interfaces 56 (2025) 105481

Contents lists available at ScienceDirect

Surfaces and Interfaces

journal homepage: www.sciencedirect.com/journal/surfaces-and-interfaces

Unveiling the role of metal-doped BNC_2 monolayer for selective gas adsorption: A DFT investigation

Audomsak Sripothongnack, Watcharin Teeranattapong, Aroon Ananchuensook [1], Thanasee Thanasarnsurapong, Jiraroj T-Thienprasert, Chatchawal Wongchoosuk, Pakpoom Reunchan [*]

Department of Physics, Faculty of Science, Kasetsart University, Bangkok 10900, Thailand

ARTICLE INFO

Keywords:
BNC_2
Doping
Gas sensor
DFT

ABSTRACT

Developing effective gas sensors is crucial for environmental monitoring, safety, and industrial applications. Two-dimensional (2D) materials are increasingly investigated as gas-sensing platforms due to their high surface-to-volume ratios and tunable electronic properties. In this study, we utilize density functional theory (DFT) to investigate the gas-sensing properties of the BNC_2 monolayer (ML), focusing on the adsorption of CO, CO_2, NO, NO_2, and HCN on pristine and metal-doped (Li, Mg, and Al) BNC_2. Our results reveal that all doped metal atoms are strongly bound to the BNC_2 surface, though slightly protruding from the plane. Among the dopants, Al-doped BNC_2 exhibits the strongest interaction with gas molecules, particularly NO and NO_2, while Mg-doped BNC_2 shows a balanced interaction, making it highly suitable for selective gas sensing. Li-doped BNC_2, in contrast, demonstrates weaker interactions, leading to faster desorption times. The charge transfer analysis indicates that most gas molecules act as charge acceptors, with NO and NO_2 showing significant electron gain from Mg- and Al-doped surfaces. Additionally, recovery time calculations suggest that metal doping significantly enhances gas-sensing performance compared to pristine BNC_2, particularly for NO and NO_2 detection. This work underscores the versatility of metal-doped BNC_2 monolayers, both in gas sensing and gas capture, contributing to the development of advanced sensing technologies and environmental sustainability solutions.

1. Introduction

Rapid transformation and development have led to significant progress worldwide in recent decades. However, this progress has also brought about environmental pollution, highlighting the need for effective environmental protection. Sensors play a crucial role in detecting various pollutants and toxic gases [1,2]. Gas sensors are essential for numerous applications, including environmental monitoring [3], industrial and military safety, [4] medical diagnosis [5], and agriculture [6]. Adsorption is key in activating gas molecules with commonly used adsorbents like zeolites [7], activated carbon [8], and metal-organic frameworks [9]. Despite their use, these materials have limitations that prevent them from fully meeting practical application requirements. Consequently, researchers are focusing on developing new, more efficient adsorbents [10–12]. The detection and monitoring of gas molecules are critical for various applications, including environmental protection, industrial safety, and public health. Harmful gases such as carbon monoxide (CO), carbon dioxide (CO_2), nitrogen monoxide (NO), nitrogen dioxide (NO_2), and hydrogen cyanide (HCN) pose significant risks due to their toxicity and potential environmental impact. Accurate and efficient gas sensors are essential for preventing exposure to these gases and mitigating their adverse effects. For instance, CO is a colorless, odorless gas that can be lethal even at low concentrations, while NO and NO_2 contribute to air pollution and respiratory problems. HCN, a highly toxic gas, is a potential threat in various industrial processes. Therefore, the development of sensitive, selective, and reliable gas sensors is of paramount importance.

Numerous two-dimensional (2D) materials have been extensively researched for their potential in gas-sensing applications [11]. These materials include graphene derivatives, [12,13] transition metal dichalcogenides (TMDs) [14,15], phosphorene [16], black phosphorus [17,18], C_xN_y-based materials [19,20], transition metal carbides and

* Corresponding author.
E-mail address: pakpoom.r@ku.ac.th (P. Reunchan).
[1] Present address: Department of Physics and Astronomy, The University of Kansas

https://doi.org/10.1016/j.surfin.2024.105481
Received 14 October 2024; Received in revised form 13 November 2024; Accepted 19 November 2024
Available online 24 November 2024

nitrides (MXenes) [15,21], and other 2D constituents [22–25]. The unique electronic and chemical properties of these materials have shown promise in detecting gases such as NO [18,22,25], NO_2 [22,24,26,27], CO [22,25,28], CO_2 [24,25,28,29], and HCN [30–32]. However, ongoing investigations are focused on optimizing the sensitivity, recyclability, and capturing ability for practical gas sensing applications.

Recently, it has been discovered that boron, nitrogen, and carbon can be combined to form B-N-C-based 2D materials, including BC_2N and its polymorphs [33–35]. Ternary configurations of $B_xC_yN_z$ have been synthesized and investigated for their potential applications in hydrogen evolution and other applications [27,36–39]. A polymorph BNC_2, with separate graphene and h-BN domain, blending the boron nitride and graphene properties, presents a promising gas adsorption and sensing platform [40–42]. Its large surface area, tunable electronic properties, and high chemical stability make BNC_2 an excellent candidate for gas sensor development. While BNC_2 monolayers are primarily studied in theoretical contexts, the experimental synthesis and stabilization of 2D monolayers typically involve using support substrates. Substrates like SiO_2, graphene, or TMDs have been successfully employed for various 2D materials, including graphene, h-BN, and BCN_2 monolayers [43,44]. These substrates help maintain the structural integrity of the monolayer, prevent folding or wrinkling, and can even enhance gas adsorption properties by inducing strain or modifying the electronic environment of the material. However, the pristine BNC_2 monolayer may have limitations in sensitivity and selectivity, which can be addressed through doping with metal atoms. Doping is a well-established strategy to enhance the gas-sensing properties of materials. Introducing foreign atoms into the host lattice can significantly modify the electronic structure and surface chemistry, improving interaction with gas molecules [11]. Previous studies have shown that doping BNC_2 with metals such as aluminum (Al) can significantly enhance its gas adsorption properties [41]. Expanding on these findings, our study investigates the effects of various metal dopants on the gas-sensing capabilities of BNC_2, offering practical implications for developing more efficient gas sensors.

In this study, we utilize density functional theory (DFT) to investigate the gas-sensing properties of monolayer BNC_2 doped with a range of metal atoms, including lithium (Li), magnesium (Mg), and aluminum (Al). These metals were chosen based on their distinct chemical properties and potential to alter the electronic characteristics of BNC_2. Our research focuses on the adsorption behavior of specific gas molecules—CO, CO_2, NO, NO_2, and HCN—on pristine and metal-doped BNC_2 monolayers. We aim to understand how different metal dopants influence the adsorption mechanisms, electronic properties, and recovery times of BNC_2, thereby identifying the most promising doped configurations for gas sensing applications. The interaction between the gas molecules and the doped BNC_2 is characterized by adsorption energy, charge transfer, and changes in electronic structure.

Additionally, we analyze the recovery times of the gas molecules at various temperatures to assess the practical feasibility of using metal-doped BNC_2 as a gas sensor. Fast recovery times are crucial for the real-time monitoring of gases, allowing the sensor to reset quickly and be ready for subsequent detection cycles. Our study provides a comprehensive understanding of the potential of metal-doped BNC_2 for gas sensing and gas capture, contributing to environmental sustainability by enabling efficient detection and removal of harmful gases from the atmosphere.

2. Computational method

Our DFT calculations were performed using the Vienna Ab initio Simulation Package (VASP) [45,46]. The exchange-correlation functional was treated with the generalized gradient approximation (GGA) as parameterized by Perdew-Burke-Ernzerhof (PBE) [47]. A plane-wave basis set with an energy cutoff of 500 eV was utilized. For Brillouin zone integration, a Monkhorst-Pack k-point mesh of $9\times3\times1$ was applied. To model the metal-doped BNC_2 and its interaction with isolated gas molecules, a supercell composed of $4\times2\times1$ repetitions of the primitive cell was constructed, with a corresponding k-point mesh of $3\times1\times1$. Van der Waals interactions were included in all calculations using the DFT-D3 method proposed by Grimme to accurately capture the interactions between the gas molecules and both pristine and doped BNC_2 [48]. All atomic positions were relaxed until the residual forces were below 0.02 eV/Å. To prevent spurious interactions between periodic supercells, a vacuum space of 20 Å was introduced in the direction normal to the BNC_2 plane. We used the PHONOPY package [49] in combination with density-functional perturbation theory (DFPT) to calculate and plot the phonon dispersion. The thermal corrections to the adsorption energies of NO molecule were calculated using VASPKIT [50].

The adsorption energy of a gas molecule on pristine and metal-doped BNC_2 is calculated using the following equation:

$$E_{ads} = E_{BNC_2+M+gas} - \left(E_{BNC_2+M} + E_{gas}\right) \quad (1)$$

where $E_{BNC_2+M+gas}$ is the total energy of the gas molecule adsorbed on the metal-doped BNC_2 surface, E_{BNC_2+M} is the total energy of the metal-doped BNC_2 sheet without the gas, and E_{gas} is the total energy of the isolated gas molecule. Negative adsorption energy indicates the gas molecule is favorably adsorbed onto the surface.

To compute the charge difference, the following equation was used:

$$\Delta\rho = \rho_{total} - \rho_{surface} - \rho_{gas} \quad (2)$$

where ρ_{total} represents the total charge density of the adsorbed system, and $\rho_{surface}$ and ρ_{gas} represent the charge densities of the isolated surface and the gas molecule, respectively. The charge difference plots were visualized with VESTA to identify charge accumulation regions (yellow) and charge depletion (cyan) [51]. This analysis provided insights into the electronic interactions and charge transfer between the gas molecules and the BNC_2 surface.

The work function was calculated for pristine and metal-doped BNC_2 monolayers in their bare state and after gas adsorption. The work function (Φ) is defined as the energy difference between the vacuum level and the Fermi level (E_{Fermi}) of the system:

$$\Phi = E_{vac} - E_{Fermi} \quad (3)$$

The vacuum level (E_{vac}) was determined by averaging the electrostatic potential in the vacuum region of the supercell. A dipole correction was applied along the direction perpendicular to the surface to eliminate the artificial dipole moment arising from the asymmetric slab setup, ensuring accurate work function calculations. The work function was computed after structural relaxation to ensure accurate electronic properties. The work function is a critical factor to consider when examining gas-sensitive mechanisms, as it indicates the material ability of the surface to bind electrons effectively [52].

The recovery time (τ) of the gas molecules desorbing from the BNC_2 surfaces was estimated using the following equation derived from transition-state theory:

$$\tau = \nu_0^{-1} \exp\left(\frac{E_{ads}}{k_B T}\right) \quad (4)$$

where E_{ads} is the adsorption energy of the gas molecule on the surface, k_B is the Boltzmann constant, T is the temperature (300 K), and ν_0 is the attempt frequency. Although ν_0 is typically assumed to be 10^{12} s^{-1} [19], here we estimated it as the average optical phonon frequencies of pristine BNC_2 which is $\sim4.5\times10^{13}$ s^{-1} for more accurate recovery times. Recovery times were evaluated for various gas molecules (CO, CO_2, NO, NO_2, and HCN) on pristine and metal-doped BNC_2 surfaces. The results provide insights into the sensor's performance at room temperature, where shorter recovery times indicate faster desorption, making the sensor more efficient for cyclic gas detection.

3. Results and discussion

The fundamental properties of BNC_2, including its electronic structure and stability, play a critical role in its suitability as a gas-sensing material. The pristine BNC_2 monolayer exhibits a unique combination of properties from both graphene and hexagonal boron nitride (h-BN) domains, resulting in a material with tunable electronic characteristics. Fig. 1(a) illustrates the atomic structure of the BNC_2 monolayer, showing a periodic arrangement of boron (B), nitrogen (N), and carbon (C) atoms. The calculated lattice constants for BNC_2 are $a = 2.49$ Å and $b = 8.68$ Å, as shown in Fig. 1(a). The average bond length between adjacent C atoms is 1.43 Å, slightly longer than the C-C bond length of 1.42 Å in graphene, likely due to the mixing of B-N atoms in the hexagonal lattice. These structural parameters reflect the influence of graphene-like and hexagonal boron nitride (h-BN) domains within the monolayer. The rectangular primitive cell of BNC_2 is defined by the primitive vectors $\vec{a}_1$ and $\vec{a}_2$, which can be virtually constructed from the primitive vectors $\vec{a}'_1 = \left(\frac{a}{2}\right)\hat{x} + \left(\frac{\sqrt{3}a}{2}\right)\hat{y}$ and $\vec{a}'_2 = \left(\frac{a}{2}\right)\hat{x} - \left(\frac{\sqrt{3}a}{2}\right)\hat{y}$ of a hexagonal structure e.g., graphene as follows: $\vec{a}_1 = \vec{a}'_1 + \vec{a}'_2 = a\hat{x}$, and $\vec{a}_2 = 2(\vec{a}'_2 - \vec{a}'_1) = 2\sqrt{3}a\hat{y}$, where a is the lattice constant of the graphene. However, for BNC_2, the calculated lattice parameters slightly deviate from a and $2\sqrt{3}a$ due to the mixture of the BN domain. The electronic band structure of BNC_2, shown in Fig. 1(b), indicates that the material exhibits an indirect bandgap of approximately 1.28 eV. The valence band maximum (VBM) is located at the (0.395, 0.000, 0.000). In contrast, the conduction band minimum (CBM) is located at (0.447, 0.500, 0.500) in the unit of reciprocal lattice vectors in the Brillouin zone, confirming the indirect nature of the bandgap, consistent with the previous calculations of BNC_2 electronic structure [53]. This indirect bandgap is an important feature for the potential application of materials in gas sensing, as it suggests that BNC_2 could exhibit different electronic responses upon adsorption of gas molecules, which can alter the band structure and hence its electrical conductivity.

The phonon dispersion curve, as illustrated in Fig. 1(c), demonstrates the dynamical stability of the BNC_2 ML. The absence of imaginary frequencies throughout the Brillouin zone corroborates the dynamical stability of BNC_2, signifying its ability to maintain structural integrity without spontaneous lattice distortions. We conducted ab initio molecular dynamic (AIMD) simulations using a Nosé-Hoover thermostat in an NVT ensemble to further assess its thermodynamic stability [54]. Fig. 1 (d) depicts the AIMD simulation outcomes at a temperature of 600 K, showcasing the temporal variation in free energy. The observed free energy stability throughout the simulation validates the thermodynamic stability of BNC_2 at elevated temperatures. This inherent stability underscores the potential applicability of BNC_2 in practical scenarios, particularly in environments that entail thermal fluctuations typical of real-world sensing applications. To further quantify this stability, we calculated the cohesive energy of the BNC_2 monolayer using the following equation:

$$E_{coh} = \frac{E_{BNC_2} - (n_B \times E_B + n_N \times E_N + n_C \times E_C)}{N} \quad (5)$$

where E_{BNC_2} is the total energy of BNC_2 monolayer, n_B, n_N, and n_C are the total numbers of boron, nitrogen, and carbon atoms in the monolayer, respectively. E_B, E_N, and E_C denote the energies of isolated B, N, and C atoms, respectively, and N is the total number of atoms of the monolayer. The calculated cohesive energy for BNC_2 is −7.39 eV, reflecting strong binding between its constituent atoms, consistent with the reported value [41]. This negative value indicates that the material is energetically favorable and structurally stable, making it well-suited to withstand external perturbations, such as thermal fluctuations. The

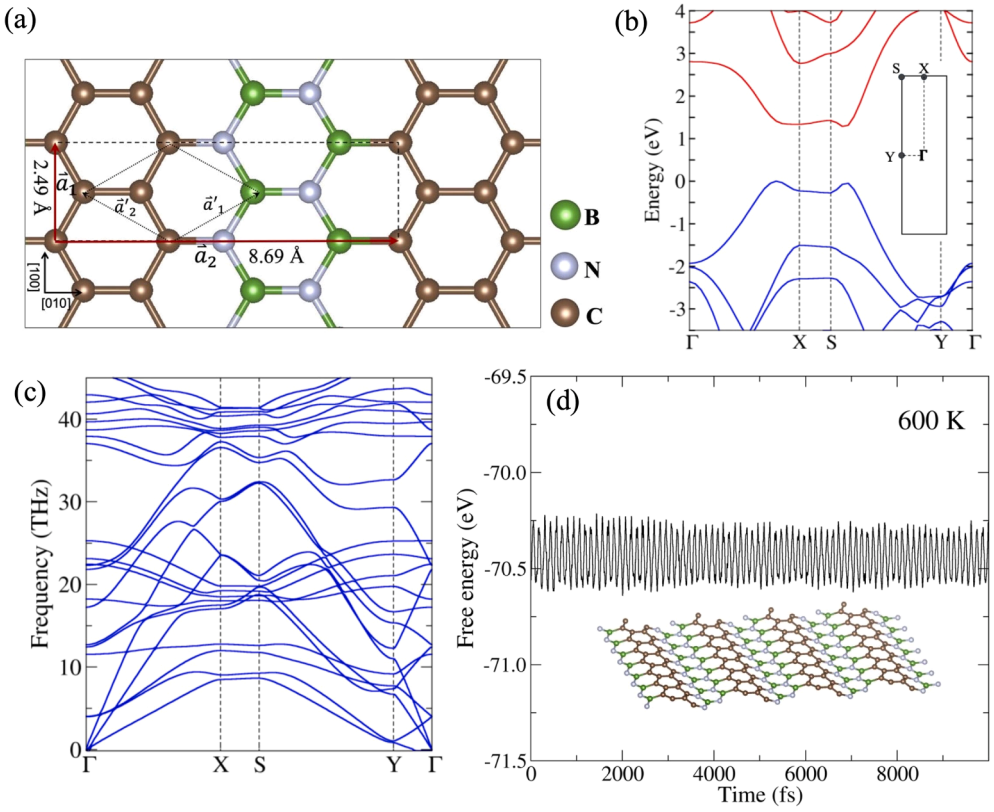

Fig. 1. (a) The primitive cell of monolayer BNC_2 consists of two B, two N, and four C atoms. (b) Electronic band structure of BNC_2. The valence band maximum is set at zero eV. The inset shows the Brillouin zone of the rectangular lattice of BNC_2. (c) Phonon dispersion curve of BNC_2. (d) Free energy profile from ab-initio molecular dynamics simulation conducted at 600 K over 10,000 fs.

result also implies that the growth of BNC_2 can be successfully achieved in real experiments.

To determine the most favorable site for metal doping in BNC_2, we calculated the cohesive energy for three different metal atoms—lithium (Li), magnesium (Mg), and aluminum (Al)—on various defect sites, including boron (B), carbon (C), and nitrogen (N) vacancies. Our cohesive energy calculations reveal that among the various defect sites investigated, the B1 site, corresponding to a boron vacancy in the BNC_2 lattice, is the most favorable for doping with lithium, aluminum, and magnesium. Although boron-nitrogen (B-N) bonds in the lattice are strong, creating a boron vacancy introduces reactivity due to dangling bonds on the adjacent nitrogen atoms. This increased reactivity enhances the binding of metal dopants, leading to a stabilized configuration with lower cohesive energy. Specifically, the cohesive energies at the B1 site are −7.24 eV for Li, −7.30 eV for Al, and −7.25 eV for Mg. These results highlight the B1 site as the most stable and favorable location for metal doping compared to other defect sites. The detailed calculations supporting this analysis are provided in the Supplementary Material (Fig. S1).

Fig. 2 presents the relaxed atomic structures of various gas molecules—CO, CO_2, NO, NO_2, and HCN—adsorbed on pristine BNC_2, with top and side views illustrating their adsorption configurations. In Fig. 2 (b) and (c), the CO and CO_2 molecules are positioned at relatively large distances of 3.24 Å and 3.10 Å from the surface, respectively. These significant separations indicate weak physisorption dominated by van der Waals forces, aligning with the low adsorption energies observed and reflecting minimal interaction with the pristine BNC_2 surface. In contrast, Fig. 2(d) and (e) show that NO and NO_2 molecules adsorb closer to the surface at distances of 2.70 Å and 2.74 Å, respectively. This suggests slightly stronger interactions, likely attributed to the polar nature of these molecules, which enhances the electrostatic attraction to the surface, though they still fall within the physisorption regime. Fig. 2 (f) reveals that HCN exhibits the closest adsorption distance at 2.57 Å, implying a stronger interaction that may involve more significant charge transfer between HCN and the BNC_2 surface.

These structural observations confirm that pristine BNC_2 primarily facilitates weak physisorption for these gases. The relatively large adsorption distances and low adsorption energies underscore the limited sensitivity of pristine BNC_2 for gas detection applications. Therefore, to enhance the interaction strength and improve gas-sensing performance, metal doping of BNC_2 is necessary, as it can modify the electronic properties of the surface and promote stronger adsorption through chemisorption mechanisms.

Now, we will explore how to enhance the gas-sensing performance of BNC_2 monolayers. The adsorption energies of various gas molecules—CO, CO_2, NO, NO_2, and HCN—were calculated on pristine BNC_2 and BNC_2 doped with Li, Mg, and Al. Fig. 3(a) illustrates the adsorption energies of various gas molecules (CO, CO_2, NO, NO_2, and HCN) on pristine and metal-doped BNC_2 monolayers with Li, Mg, and Al dopants. The numerical values of the adsorption energies are also listed in Table S2.

The adsorption energies on pristine BNC_2 are relatively low, ranging from –0.128 eV for CO to –0.257 eV for HCN. This indicates physisorption dominated by van der Waals interactions, evident by the minimal overlapping between the projected density of states (PDOS) between the molecule and the BNC_2 monolayer. This suggests that pristine BNC_2 has limited sensitivity for gas detection applications due to its minimal interaction with gas molecules. Upon doping with Li, there is a noticeable increase in adsorption energies for all gases. For instance, the adsorption energy of NO_2 increases from –0.247 eV on pristine BNC_2 to –0.588 eV on Li-BNC_2. Similarly, HCN shows an increase from –0.257 eV to –0.472 eV upon Li doping. This enhancement can be attributed to the introduction of Li atoms, which alter the electronic properties of the BNC_2 monolayer and create new active sites for adsorption. The moderate increase suggests improved sensitivity while maintaining manageable desorption rates, which is beneficial for sensor performance.

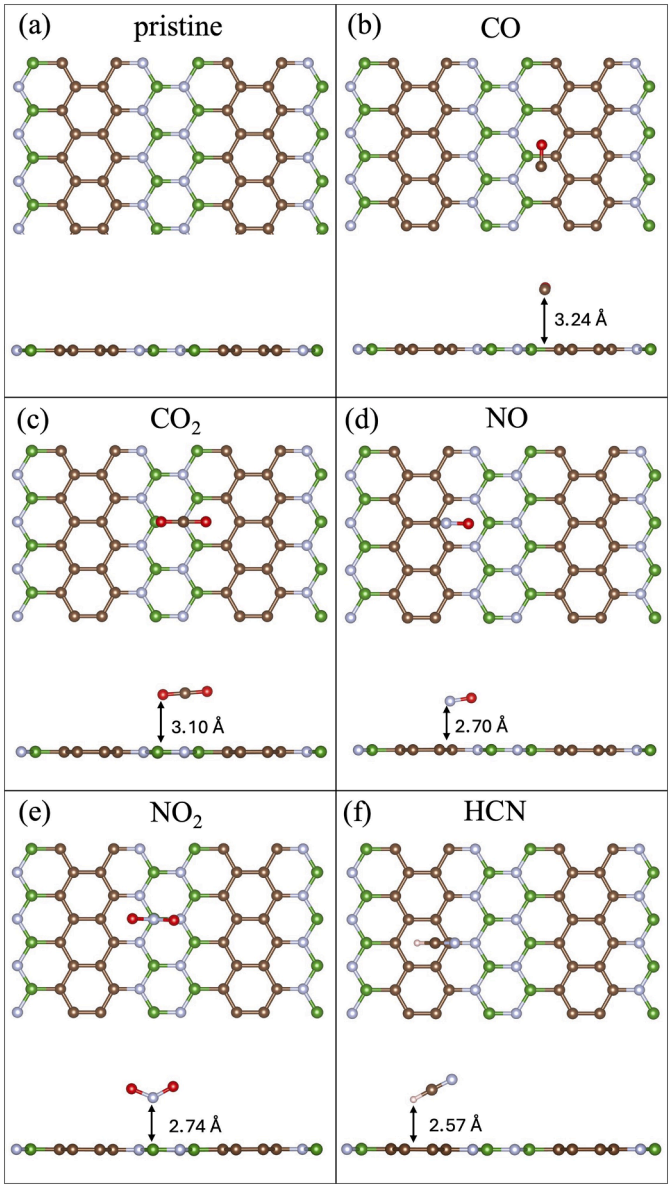

Fig. 2. Relaxed atomic structures of gas molecules (CO, CO_2, NO, NO_2, and HCN) adsorbed on pristine BNC2, presented in top and side views. The distances between the molecules and the surface indicate the strength of interaction: (a) Pristine BNC_2, (b) CO at 3.24 Å, (c) CO_2 at 3.10 Å, (d) NO at 2.70 Å, (e) NO_2 at 2.74 Å, and (f) HCN at 2.57 Å.

Mg doping leads to a more significant increase in adsorption energies. NO and NO_2 show substantial enhancements, with adsorption energies of –0.951 eV and –1.977 eV, respectively, on Mg-BNC_2. HCN also exhibits a significant increase to –0.919 eV on Mg-BNC_2. This indicates a transition from physisorption to chemisorption, implying stronger interactions and higher sensitivity for these gas molecules. Along with improved adsorption energy, chemisorption is characterized by a substantial overlap between the PDOS of the chemisorbed molecule and the substrate near the Fermi level (Fig. 6). The strong adsorption of NO_2 and HCN suggests that Mg-BNC_2 could be highly effective in detecting these pollutants, which have considerable environmental and health impacts.

Al doping results in the most pronounced enhancement across all gases studied. The adsorption energy of NO_2 reaches –2.897 eV on Al-BNC_2, indicating very strong chemisorption. HCN also shows substantial

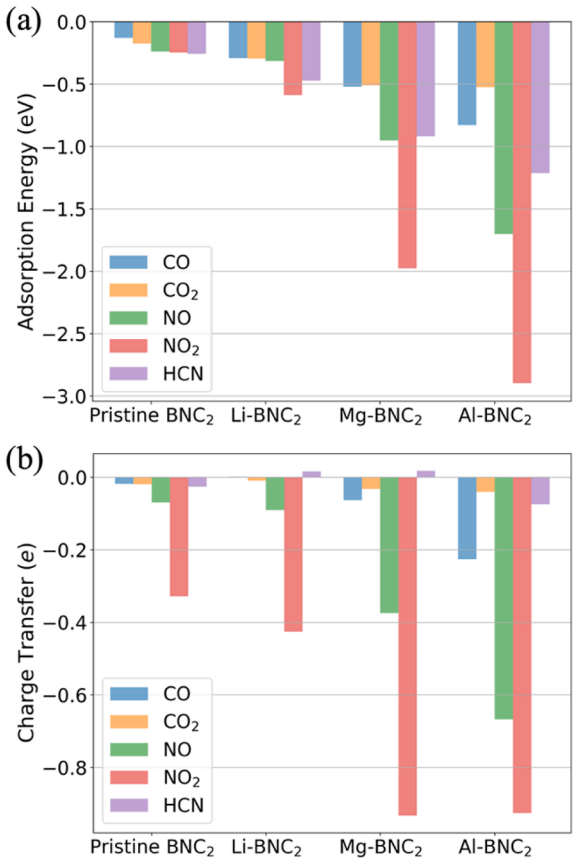

Fig. 3. (a) Adsorption energies of various gas molecules (CO, CO_2, NO, NO_2, and HCN) on pristine and metal-decorated (Li, Mg, Al) BNC_2 monolayers. (b) Charge transfer (in electron charge, *e*) between various gas molecules (CO, CO_2, NO, NO_2, and HCN) and pristine or metal-doped BNC_2 monolayers (Li, Mg, Al). Negative values indicate electron gain by the gas molecule from the BNC_2 surface, while positive values indicate electron loss by the gas molecule to the surface.

adsorption energy of –1.213 eV on Al-BNC_2. While this suggests exceptional sensitivity, the strong binding may pose challenges for sensor recovery and reusability due to slow desorption rates. Therefore, while Al-BNC_2 shows potential for gas capture applications, its practicality in sensing devices may require further investigation to balance sensitivity with operational efficiency.

The trends observed indicate that metal doping significantly enhances the interaction between gas molecules and the BNC_2 monolayer. The increase in adsorption energies follows the order of the dopant's ability to alter the electronic structure of BNC_2: Al > Mg > Li. This enhancement is particularly notable for gases like NO, NO_2, and HCN, which are known to have higher environmental and health impacts. In contrast, CO and CO_2 exhibit smaller increases in adsorption energies upon doping. Even with Al doping, the adsorption energies for CO (–0.829 eV) and CO_2 (–0.525 eV) are lower than those of NO, NO_2, and HCN. This suggests that metal-doped BNC_2 monolayers own high selectivity toward certain gas molecules, which is advantageous for applications requiring specific gas detection without interference from others.

To assess the impact of thermal effects on the adsorption energies, we calculated the zero-point vibrational energy (ZPVE) and entropy contributions at 300 K for the adsorption of NO on pristine and metal-doped BNC_2 surfaces (Li, Mg, and Al) as a representative case. The thermal corrections were minimal, amounting to less than 0.02 eV across all surfaces. This negligible contribution arises from the small changes in vibrational frequencies upon adsorption and the limited entropy change, as the NO molecule vibrational modes are not significantly altered when adsorbed. Based on these observations, we expect the thermal corrections for other gas molecules studied—CO, CO_2, NO_2, and HCN—to be negligible due to their comparable adsorption mechanisms and vibrational properties. Consequently, the adsorption energies presented in this work are predominantly determined by electronic interactions, and the minor thermal corrections do not substantially affect the adsorption thermodynamics or the conclusions regarding the gas-sensing capabilities of pristine and metal-doped BNC_2 monolayers.

The Bader charge analysis provides insights into the interactions between gas molecules and the BNC_2 surfaces [55]. As presented in Fig. 3(b), the charge transfer values reveal that metal doping significantly influences the amount of charge exchanged during adsorption. Pristine BNC_2 exhibits minimal charge transfer with all gases studied, indicating weak physisorption interactions. The charge transfer magnitudes generally increase upon doping with Li, Mg, or Al, especially for NO and NO_2, suggesting that metal doping enhances the electronic interactions between the gas molecules and the surface. Notably, NO_2 shows the largest negative charge transfer across all doped surfaces, with values of $-0.426e$ on Li-BNC_2, $-0.932e$ on Mg-BNC_2, and $-0.925e$ on Al-BNC_2. This substantial electron transfer from NO_2 to the surface indicates strong chemisorption, correlating with the previously calculated adsorption energies. Similarly, NO exhibits significant charge transfer, particularly on Mg- and Al-doped BNC_2, further confirming the strong interaction and potential for high sensitivity in detecting these gases.

In contrast, CO and CO_2 display much smaller charge transfers, even on doped surfaces. For example, CO transfers only $-0.063e$ on Mg-BNC_2 and $-0.226e$ on Al-BNC_2. These lower values correspond to the weaker adsorption energies and shorter recovery times observed for these gases, indicating that while they interact more strongly with doped surfaces than with pristine BNC_2, the interaction is still relatively weak compared to NO and NO_2. The varying charge transfer behaviors among different gases highlight the potential for selective gas sensing using metal-doped BNC_2 monolayers. The significant charge transfer associated with NO and NO_2 adsorption on Mg- and Al-doped BNC_2 suggests that these materials could serve as highly sensitive sensors for nitrogen oxides. Conversely, the relatively low charge transfer with CO and CO_2 indicates that these gases would have a lesser impact on the sensor's electrical properties, reducing the likelihood of interference and false positives. The relatively high adsorption energy observed for the HCN molecule, despite a modest overall charge transfer, can be attributed to localized charge transfer on specific atoms within the molecule. Specifically, the N atom of HCN, which is adjacent to the adsorption site (Li, Mg, or Al atom), exhibits a notable gain of electrons (negative charge transfer), while the H atoms display a significant loss of electrons (positive charge transfer). These opposing charge transfers contribute to the overall stability of the adsorption configuration. Detailed numerical values of the charge transfer on individual atoms in the adsorbed molecules and the total charge transfer are provided in Tables S3–S8 in the Supplementary Material.

Fig. 4 illustrates the work function for pristine and metal-doped BNC_2 surfaces (Li, Mg, and Al doping) in their bare state and after the adsorption of various gas molecules (CO, CO_2, NO, NO_2, and HCN). The work function, which is a key parameter reflecting the electronic properties of a surface, changes upon gas adsorption, providing critical insights into the interaction strength and charge transfer processes between the gas molecules and the BNC_2 surfaces. The results show that the work function shifts are relatively small for CO and CO_2 adsorption across all surfaces, indicating weaker interactions and minimal charge transfer. This aligns with the low adsorption energies and charge transfer values in Fig. 3(a) and (b), suggesting weak interaction with pristine and doped BNC_2 surfaces. In contrast, significant increases in the work function are observed for NO and NO_2, especially on Mg- and Al-doped BNC_2. For example, the work function for NO_2 increases from 4.28 eV to 5.36 eV on Al-doped BNC_2, which correlates with substantial

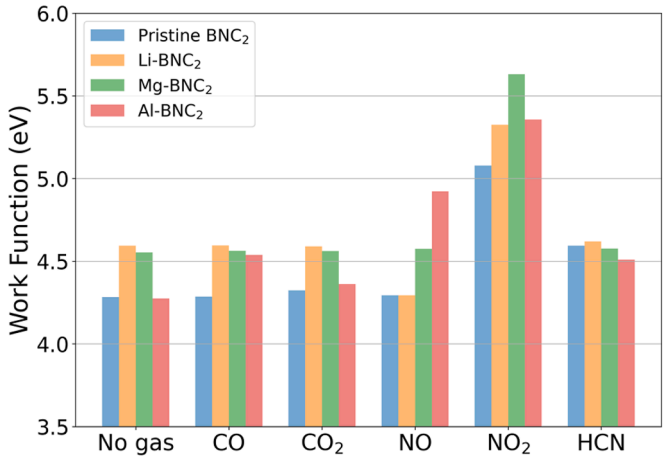

Fig. 4. Work function for pristine BNC_2 and metal-doped BNC_2 surfaces (Li, Mg, and Al) both in their bare state and after the adsorption of various gas molecules (CO, CO_2, NO, NO_2, and HCN).

charge transfer and strong adsorption energies noted in Fig. 3. These findings suggest a robust interaction between these gases and the surface, where the adsorbed molecules significantly alter the electronic structure, indicating enhanced surface sensitivity to these gases.

While HCN also causes moderate charge transfer, the resulting work function shifts are less pronounced, especially on Mg- and Al-doped surfaces. This suggests that although HCN interacts with the surface, its impact on the electronic properties is less significant than that of NO and NO_2. This behavior aligns with its intermediate adsorption energy and charge transfer values, positioning it between the weakly interacting CO and the strongly interacting NO_2.

Fig. 5 presents the charge difference plots for Mg-doped BNC_2 upon adsorption of various gas molecules, showing charge redistribution across the surface. The plots reveal that NO and NO_2 induce the most significant charge accumulation near the gas molecules, particularly around the oxygen and nitrogen atoms, coupled with substantial charge depletion near the Mg atom. These observations are consistent with the high adsorption energies and large charge transfer values observed for these gases, highlighting the strong interaction between NO_2 and NO with the Mg-doped surface. In contrast, CO and CO_2 show more moderate charge redistribution, with weaker electron transfer, as reflected in their lower adsorption energies. HCN exhibits intermediate behavior, with moderate charge accumulation around the nitrogen atom, indicating a somewhat stronger interaction than CO but weaker than NO and NO_2. These results confirm that Mg-doped BNC_2 is highly reactive toward NO and NO_2, making it a promising material for gas-sensing applications while showing weaker interaction with CO and CO_2. The charge redistribution in Mg-doped BNC_2 is more pronounced than in Li-doped BNC_2 (see Supplementary Material, Fig. S2), suggesting stronger gas-surface interactions. However, compared to Al-doped BNC_2 (Fig. S3), the charge redistribution is less intense, reflecting the intermediate adsorption energy and charge transfer values for Mg doping. This moderate behavior highlights the tunability of the BNC_2 surface through different dopants, with Mg providing a balance between reactivity and stability.

The density of states (DOS) plots in Fig. 6 reveal key insights into the interactions between Mg-doped BNC_2 and various gas molecules, with the Fermi level set at 0 eV. For the Mg-doped BNC_2 system (Fig. 6(a)), the Fermi level lies slightly below the valence band, indicating semiconducting behavior. Upon gas adsorption, the position of the projected density of states (PDOS) of the gas molecules relative to the Fermi level reflects the degree of charge transfer and the strength of interaction between the gas and the Mg-doped surface.

For CO adsorption (Fig. 6(b)), the PDOS shows that CO introduces

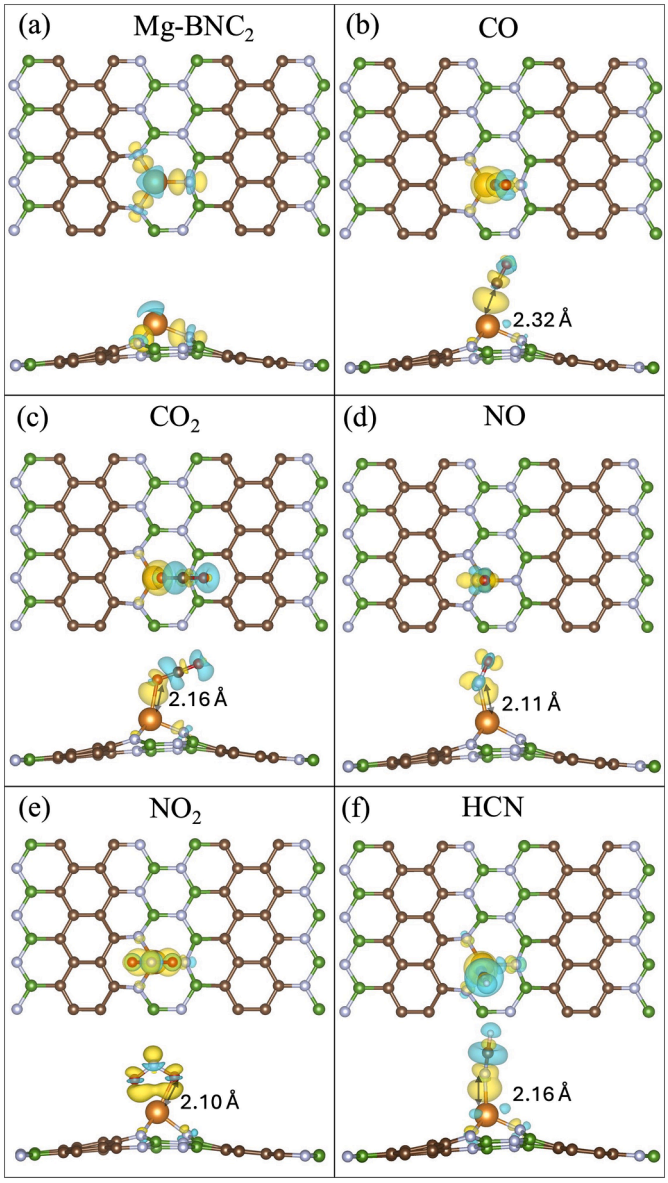

Fig. 5. Charge difference plots for Mg-doped BNC_2 upon adsorption of various gas molecules: (a) pristine Mg-doped BNC_2, (b) CO, (c) CO_2, (d) NO, (e) NO_2, and (f) HCN. Yellow and cyan regions represent charge accumulation and charge depletion, respectively. The adsorption distances between the gas molecules and the surface are indicated. The isosurface of the charge distribution was set to 10% of the maximum.

molecular states close to the Fermi level, indicating relatively strong interaction and significant charge transfer from the surface to the CO molecule. This observation is consistent with the charge transfer in Fig. 3 (b), where CO gains a noticeable amount of charge ($-0.063e$) from the Mg-doped surface. The appearance of states near the Fermi level suggests that CO interacts more strongly with the surface than CO_2, further supported by its moderate adsorption energy and slower recovery time compared to CO_2. In contrast, the CO_2 PDOS (Fig. 6(c)) shows molecular states more distant from the Fermi level, notably higher in the conduction band, which indicates a weaker interaction with the surface. The corresponding charge transfer value for CO_2 ($-0.032e$) in Fig. 3(b) reflects this reduced charge transfer, supporting the conclusion that CO_2 interacts less strongly with Mg-doped BNC_2 than CO. The weaker adsorption also aligns with the faster recovery time observed for CO_2.

The interaction is much stronger for NO and NO_2 (Fig. 6(d) and (e)), as both gases introduce significant molecular states near and below the

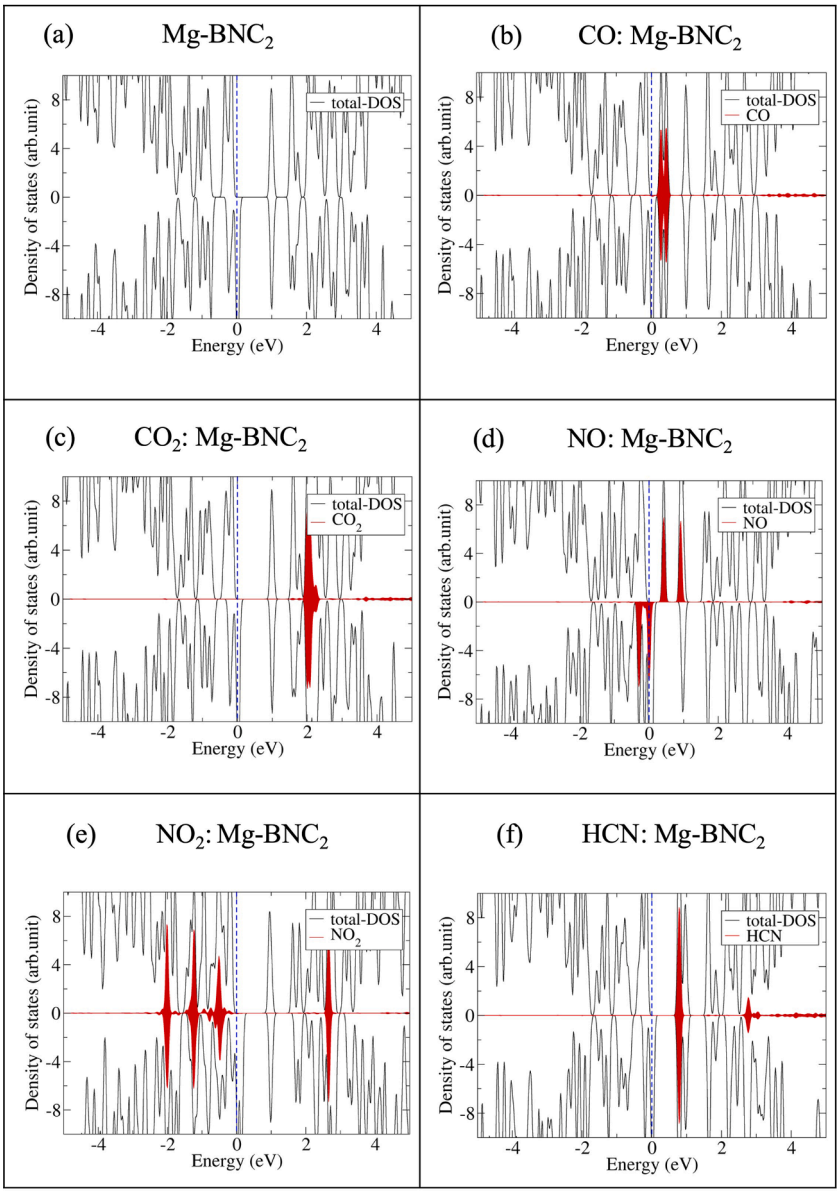

Fig. 6. Total density of states (DOS) for Mg-doped BNC_2 (a) and gas adsorbed systems: (b) CO, (c) CO_2, (d) NO, (e) NO_2, and (f) HCN. The black line represents the total DOS of the system, and the red line represents the projected DOS of the adsorbed gas molecules. The vertical dashed line at 0 eV indicates the Fermi level.

Fermi level. These states suggest substantial charge transfer from the surface to the gas molecules, as confirmed by the charge transfer data in Fig. 3(b), where NO ($-0.374e$) and NO_2 ($-0.932e$) show the largest electron gains among the studied gases. This strong interaction is consistent with the high adsorption energies and the exceptionally long recovery times observed for these gases, especially NO_2. The DOS and charge transfer results indicate that NO and NO_2 heavily modify the electronic structure of the surface, making them prime candidates for effective gas capture on Mg-doped BNC_2.

Finally, For HCN adsorption (Fig. 6(f)), the molecular states appear above the Fermi level, indicating that HCN donates electrons to the Mg-doped BNC_2 surface. States above the Fermi level are unoccupied, suggesting that the interaction is relatively weak compared to gases with states below the Fermi level. This is consistent with the positive charge transfer value shown in Fig. 3(b) ($+0.018e$), meaning that HCN loses electrons to the surface. The position of the HCN states above the Fermi level correlates with its moderate adsorption energy and recovery time, suggesting that while HCN binds to the surface, the interaction is weaker than that of gases like NO or NO_2, which exhibit stronger charge transfer and deeper molecular states near the Fermi level. In addition to Mg-doped BNC_2, the electronic structure and gas adsorption behavior for Li- and Al-doped BNC_2 were also studied. The corresponding density of states (DOS) plots for Li- and Al-doped systems are provided in the Supplementary Material (Fig. S4-S5), showing trends consistent with the charge transfer and adsorption energy analyses discussed earlier.

Sensitivity in gas-sensing applications is closely linked to changes in the electronic properties of the sensing material upon gas adsorption [56–58]. In addition to adsorption energy and charge transfer, which provide insight into the interaction strength and electronic response, recent studies suggest that sensitivity can also be estimated by observing changes in the band gap. The sensitivity S can be estimated by the equation $S = |\exp\left(\frac{E_g^f - E_g^i}{2kT}\right) - 1|$ where E_g^i and E_g^f represents the band gap before (E_g^i) and after (E_g^f) gas adsorption [59], estimated from the DOS plots. This method allows for a qualitative assessment of the sensor response to gas molecules, especially in cases where adsorption induces notable band structure modifications. Our estimated sensitivity values

for the five gases on Mg-doped BNC_2 at room temperature (kT=0.0259 eV), while neglecting a slight change in band gap with temperature, are shown in Table 1. The results in Table 1 indicate that the sensitivity of each molecule varies and qualitatively aligns with the adsorption energy and charge transfer reported earlier.

Fig. 7 presents the recovery times of various gas molecules—CO, CO_2, NO, NO_2, and HCN—on pristine and metal-doped BNC_2 surfaces (doped with Li, Mg, and Al) at 300 K, using an attempt frequency of 4.5×10^{13} Hz. On pristine BNC_2, all gases exhibit extremely short recovery times, ranging from 10^{-10} to 10^{-9} seconds, indicating weak interactions and rapid desorption unsuitable for effective gas sensing due to low sensitivity. Li-doped BNC_2 shows slightly longer recovery times, particularly for NO_2 (4.0×10^{-4} s), but these are still relatively short, suggesting that Li doping only marginally enhances gas interactions. In contrast, Mg-doped BNC_2 displays significantly stronger adsorption, with NO exhibiting a recovery time of 7.4×10^{2} s, making it a promising candidate for NO detection. However, NO_2 on Mg-doped BNC_2 has an excessively long recovery time of 4.9×10^{20} s, indicating overly strong binding that may hinder sensor reusability. Al-doped BNC_2 demonstrates even longer recovery times for NO (8.5×10^{15} s) and NO_2 (4.7×10^{36} s), rendering it impractical for reusable sensors.

Interestingly, CO and CO_2 on Mg- and Al-doped surfaces show much faster desorption, highlighting the potential for selective sensing. These observations suggest that sensor sensitivity and selectivity can be fine-tuned by choosing the appropriate dopant. Mg-doped BNC_2 offers a good balance for gases like NO and HCN, while Li and Al doping alter the sensor's performance in contrasting ways. For example, Li provides minimal enhancement, whereas Al causes excessively strong adsorption.

Short recovery times indicate rapid desorption, which is advantageous for gas-sensing applications requiring quick sensor reset. However, the unusually long recovery times observed for gases like NO and NO_2 on Mg- and Al-doped BNC_2 suggest a potential application in gas capture. The extremely slow desorption of these gases, with recovery times ranging from 10^{20} to 10^{36} seconds, indicates strong retention on the surface. This characteristic is highly desirable for gas capture applications that require long-term trapping of harmful gases. Therefore, metal-doped BNC_2, particularly with Mg or Al doping, could effectively capture toxic gases like NO_2, contributing to environmental remediation efforts or industrial gas sequestration.

4. Conclusion

In this study, we investigated the adsorption behavior, charge transfer, and recovery time of various gas molecules (CO, CO_2, NO, NO_2, and HCN) on pristine and Li-, Mg-, and Al-doped BNC_2 monolayers using DFT calculations. Our findings reveal that metal doping significantly enhances the interaction strength between the gas molecules and the BNC_2 surface, with Mg- and Al-doped BNC_2 showing particularly strong adsorption for NO and NO_2. The charge transfer analysis further supports these results, demonstrating substantial electron transfer in the case of NO_2 and NO, indicating strong surface-molecule interactions. In contrast, Li-doped BNC_2 displays weaker interactions and faster recovery times, making it more suited for cyclic gas sensing applications where rapid desorption is necessary.

The analysis of recovery time also emphasizes the potential of metal-doped BNC_2 monolayers, especially Mg- and Al-doped versions, for gas capture. The extended recovery times observed for NO_2 and NO on these surfaces indicate that these gases could be effectively trapped. This makes metal-doped BNC_2 a promising material for environmental clean-up or gas storage. In general, this study shows that by adjusting the dopant on the BNC_2 surface, the sensitivity of material and selectivity for gas detection and capture can be tailored, offering flexibility in various gas sensing and trapping applications.

Table 1
Percentage selectivity (S) for the CO, CO_2, NO, NO_2, and HCN molecules on Mg-doped BNC_2.

Gas	CO	CO_2	NO	NO_2	HCN
S (%)	49.64	31.73	92.55	94.41	98.13

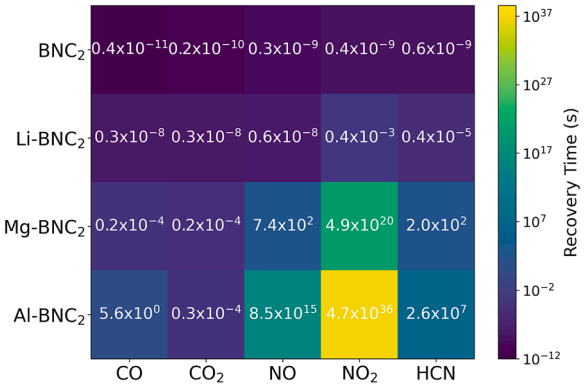

Fig. 7. Recovery times of various gas molecules (CO, CO_2, NO, NO_2, and HCN) on pristine and metal-doped BNC_2 surfaces (Li, Mg, and Al) at 300 K, using an attempt frequency of 4.5×10^{13} Hz. The color scale represents the recovery time in seconds, ranging from 10^{-12} to 10^{37} seconds.

CRediT authorship contribution statement

Audomsak Sripothongnack: Writing – original draft, Visualization, Investigation, Formal analysis. **Watcharin Teeranattapong:** Visualization, Investigation. **Aroon Ananchuensook:** Visualization, Methodology, Investigation. **Thanasee Thanasarnsurapong:** Validation, Methodology, Investigation. **Jiraroj T-Thienprasert:** Writing – review & editing, Validation, Investigation. **Chatchawal Wongchoosuk:** Writing – review & editing, Validation, Investigation. **Pakpoom Reunchan:** Writing – review & editing, Writing – original draft, Supervision, Investigation, Conceptualization, Funding acquisition.

Declaration of competing interest

The authors declare that they have no known competing financial interests or personal relationships that could have appeared to influence the work reported in this paper.

Acknowledgment

This work was supported by the Kasetsart University Research and Development Institute (KURDI) through Fundamental Funds (FF(KU) 8.68). A.S. thanks the Faculty of Science, Kasetsart University, for the support through the Undergraduate Research Matching Fund. P.R. acknowledges the NSRF via the Program Management Unit for Human Resources & Institutional Development, Research, and Innovation [grant number B39G670019]. We thank the NSTDA Supercomputer Center (ThaiSC) for providing computing resources for this work.

Supplementary materials

Supplementary material associated with this article can be found, in the online version, at doi:10.1016/j.surfin.2024.105481.

Data availability

Data will be made available on request.

References

[1] S. Dhall, B.R. Mehta, A.K. Tyagi, K. Sood, A review on environmental gas sensors: materials and technologies, Sens. Int. 2 (2021) 100116.
[2] V. Balasubramani, S. Chandraleka, T.S. Rao, R. Sasikumar, M.R. Kuppusamy, T. M. Sridhar, Review—recent advances in electrochemical impedance spectroscopy based toxic gas sensors using semiconducting metal oxides, J. Electrochem. Soc. 167 (2020) 037572.
[3] T. Seesaard, K. Kamjornkittikoon, C. Wongchoosuk, A comprehensive review on advancements in sensors for air pollution applications, Sci. Total Environ. 951 (2024) 175696.
[4] M.F.R. Al-Okby, S. Neubert, T. Roddelkopf, K. Thurow, Mobile detection and alarming systems for hazardous gases and volatile chemicals in laboratories and industrial locations, Sensors 21 (2021) 8128.
[5] A.A. Ghawanmeh, S. A.Tanash, N.A.F. Al-Rawashdeh, B. Albiss, The recent progress on nanomaterial-based chemosensors for diagnosis of human exhaled breath: a review, J. Mater. Sci. 59 (2024) 8573–8605.
[6] T. Seesaard, N. Goel, M. Kumar, C. Wongchoosuk, Advances in gas sensors and electronic nose technologies for agricultural cycle applications, Comput. Electron. Agric. 193 (2022) 106673.
[7] K. Sahner, G. Hagen, D. Schönauer, S. Reiß, R. Moos, Zeolites — Versatile materials for gas sensors, Solid. State Ion. 179 (2008) 2416–2423.
[8] N.A. Travlou, M. Seredych, E. Rodríguez-Castellón, T.J. Bandosz, Activated carbon-based gas sensors: effects of surface features on the sensing mechanism, J. Mater. Chem. A 3 (2015) 3821–3831.
[9] H.-Y. Li, S.-N. Zhao, S.-Q. Zang, J. Li, Functional metal–organic frameworks as effective sensors of gases and volatile compounds, Chem. Soc. Rev. 49 (2020) 6364–6401.
[10] E. Llobet, Gas sensors using carbon nanomaterials: a review, Sens. Actuat. B Chem. 179 (2013) 32–45.
[11] S. Yang, C. Jiang, S.-h. Wei, Gas sensing in 2D materials, Appl. Phys. Rev. 4 (2017).
[12] S. Gupta Chatterjee, S. Chatterjee, A.K. Ray, A.K. Chakraborty, Graphene–metal oxide nanohybrids for toxic gas sensor: a review, Sens. Actuat. B Chem. 221 (2015) 1170–1181.
[13] R. Ghosh, M. Aslam, H. Kalita, Graphene derivatives for chemiresistive gas sensors: A review, Mater. Today Commun. 30 (2022) 103182.
[14] W. Zheng, X. Liu, J. Xie, G. Lu, J. Zhang, Emerging van der Waals junctions based on TMDs materials for advanced gas sensors, Coord. Chem. Rev. 447 (2021) 214151.
[15] A. Mirzaei, J.-Y. Kim, H.W. Kim, S.S. Kim, Resistive gas sensors based on 2D TMDs and MXenes, Acc. Chem. Res. 57 (2024) 2395–2413.
[16] S. Cui, H. Pu, S.A. Wells, Z. Wen, S. Mao, J. Chang, M.C. Hersam, J. Chen, Ultrahigh sensitivity and layer-dependent sensing performance of phosphorene-based gas sensors, Nat. Commun. 6 (2015) 8632.
[17] A.N. Abbas, B. Liu, L. Chen, Y. Ma, S. Cong, N. Aroonyadet, M. Köpf, T. Nilges, C. Zhou, Black phosphorus gas sensors, ACS. Nano 9 (2015) 5618–5624.
[18] T. Wang, X. Li, J. Wang, L. Li, D. Li, Two-dimension black arsenic-phosphorus as a promising NO sensor: A DFT study, Comput. Theor. Chem. 1213 (2022) 113727.
[19] Y. Yong, H. Cui, Q. Zhou, X. Su, Y. Kuang, X. Li, C2N monolayer as NH3 and NO sensors: A DFT study, Appl. Surf. Sci. 487 (2019) 488–495.
[20] M. Chen, H. Zhang, H. Li, Z. Zhao, K. Wang, Y. Zhou, X. Zhao, D.P. Dubal, CxNy-based materials as gas sensors: Structure, performance, mechanism and perspective, Coord. Chem. Rev. 503 (2024) 215653.
[21] B. Zhao, X. Liu, J. Su, C. Liu, Y. Feng, T. Shen, Adsorption and potential CO gas-sensing performance of the Fe-Doped Ti2CO2-MXenes: a first-principles study, Langmuir. (2024).
[22] M.I. Khan, M. Hassan, A. Majid, M. Shakil, M. Rafique, DFT perspective of gas sensing properties of Fe-decorated monolayer antimonene, Appl. Surf. Sci. 616 (2023) 156520.
[23] V. Shukla, J. Wärnå, N.K. Jena, A. Grigoriev, R. Ahuja, Toward the realization of 2D borophene based gas sensor, J. Phys. Chem. C 121 (2017) 26869–26876.
[24] V. Kumar, D.R. Roy, Single-layer stanane as potential gas sensor for NO2, SO2, CO2 and NH3 under DFT investigation, Physica E: Low-dimension. Syst. Nanostruct. 110 (2019) 100–106.
[25] B.A. Kalwar, W. Fangzong, A.M. Soomro, M.R. Naich, M.H. Saeed, I. Ahmed, Highly sensitive work function type room temperature gas sensor based on Ti doped hBN monolayer for sensing CO2, CO, H2S, HF and NO. A DFT study, RSC. Adv. 12 (2022) 34185–34199.
[26] A. Kumar, N. Sharma, A.P. Gutal, D. Kumar, P. Kumar, M. Paranjothy, M. Kumar, Growth and NO2 gas sensing mechanisms of vertically aligned 2D SnS2 flakes by CVD: Experimental and DFT studies, Sens. Actuat. B Chem. 353 (2022) 131078.
[27] I. Rhrissi, A. Bouhmouche, I. Abdelrhafor, R. Moubah, Strain-engineered 2D h-BC2N monolayer as a potential gas sensor with exceptional sensitivity and selectivity for NO2 gas detection, Mater. Sci. Semicond. Process. 182 (2024) 108707.
[28] E. Salih, A.I. Ayesh, Pt-doped armchair graphene nanoribbon as a promising gas sensor for CO and CO2: DFT study, Physica E: low-dimensional systems and nanostructures 125 (2021) 114418.
[29] T. Alaa Hussein, N.M. Shiltagh, W. Kream Alaarage, R.R. Abbas, R.A. Jawad, A. H. Abo Nasria, Electronic and optical properties of the BN bilayer as gas sensor for CO2, SO2, and NO2 molecules: A DFT study, Results. Chem. 5 (2023) 100978.
[30] F. Opoku, P.P. Govender, Two-dimensional CoOOH as a highly sensitive and selective H2S, HCN and HF gas sensor: a computational investigation, Electroanalysis. 32 (2020) 2764–2774.
[31] S. Cheng, J. Chen, W. Zeng, Q. Zhou, The adsorption and sensing mechanism of toxic gases HCN, NO2, NH3 and Cl2 on Mo, Ag-modified WSe2 monolayer: Insights from the first-principles computations, Mater. Today Commun. 35 (2023) 105906.
[32] S. Cai, Q. Zhou, Z. Zhao, X. Liu, W. Ju, J. Hou, Density functional theory analysis of the sensitivity of silicene/graphene heterostructures toward HCN, Colloids Surf. A Physicochem. Eng. Aspects 681 (2024) 132799.
[33] M.O. Watanabe, S. Itoh, K. Mizushima, T. Sasaki, Bonding characterization of BC2N thin films, Appl. Phys. Lett. 68 (1996) 2962–2964.
[34] L. Ci, L. Song, C. Jin, D. Jariwala, D. Wu, Y. Li, A. Srivastava, Z.F. Wang, K. Storr, L. Balicas, F. Liu, P.M. Ajayan, Atomic layers of hybridized boron nitride and graphene domains, Nat. Mater. 9 (2010) 430–435.
[35] T.H. Seo, W. Lee, K.S. Lee, J.Y. Hwang, D.I. Son, S. Ahn, H. Cho, M.J. Kim, Dominant formation of h-BC2N in h-BxCyNz films: CVD synthesis and characterization, Carbon. N. Y. 182 (2021) 791–798.
[36] C.N.R. Rao, M. Chhetri, Borocarbonitrides as metal-free catalysts for the hydrogen evolution reaction, Adv. Mater. 31 (2019) 1803668.
[37] M. Chhetri, S. Maitra, H. Chakraborty, U.V. Waghmare, C.N.R. Rao, Superior performance of borocarbonitrides, BxCyNz, as stable, low-cost metal-free electrocatalysts for the hydrogen evolution reaction, Energy Environ. Sci. 9 (2016) 95–101.
[38] C.N.R. Rao, K. Gopalakrishnan, Borocarbonitrides, BxCyNz: synthesis, characterization, and properties with potential applications, ACS. Appl. Mater. Interfaces. 9 (2017) 19478–19494.
[39] N. kumar, K. Moses, K. Pramoda, S.N. Shirodkar, A.K. Mishra, U.V. Waghmare, A. Sundaresan, C.N.R. Rao, Borocarbonitrides, BxCyNz, J. Mater. Chem. A 1 (2013) 5806–5821.
[40] S. Beniwal, J. Hooper, D.P. Miller, P.S. Costa, G. Chen, S.-Y. Liu, P.A. Dowben, E.C. H. Sykes, E. Zurek, A. Enders, Graphene-like Boron–Carbon–Nitrogen monolayers, ACS. Nano 11 (2017) 2486–2493.
[41] P. Chalase, S. Deshpande, S. Kumavat, M. Deshpande, Adsorption mechanism of different toxic gases onto pristine BNC2 and Al-doped BNC2 monolayers, Phys. Chem. Chem. Phys. 25 (2023) 17337–17351.
[42] P. Srivastava, M. Deshpande, P. Sen, First-principles study of electronic and magnetic properties of transition metal adsorbed h-BNC2 sheets, Phys. Chem. Chem. Phys. 13 (2011) 21593–21599.
[43] M. Kaur, K. Singh, A. Vij, A. Kumar, Recent insights into BCN nanomaterials – synthesis, properties and applications, New J. Chem. 47 (2023) 2137–2160.
[44] K. Zhang, Y. Feng, F. Wang, Z. Yang, J. Wang, Two dimensional hexagonal boron nitride (2D-hBN): synthesis, properties and applications, J. Mater. Chem. C 5 (2017) 11992–12022.
[45] G. Kresse, J. Furthmüller, Efficiency of ab-initio total energy calculations for metals and semiconductors using a plane-wave basis set, Comput. Mater. Sci. 6 (1996) 15–50.
[46] G. Kresse, J. Hafner, Ab initio molecular dynamics for liquid metals, Phys. Rev. B 47 (1993) 558–561.
[47] J.P. Perdew, K. Burke, M. Ernzerhof, Generalized Gradient Approximation Made Simple, Phys. Rev. Lett. 77 (1996) 3865–3868.
[48] S. Grimme, J. Antony, S. Ehrlich, H. Krieg, A consistent and accurate ab initio parametrization of density functional dispersion correction (DFT-D) for the 94 elements H-Pu, J. Chem. Phys. 132 (2010) 154104.
[49] A. Togo, I. Tanaka, First principles phonon calculations in materials science, Scr. Mater. 108 (2015) 1–5.
[50] V. Wang, N. Xu, J.-C. Liu, G. Tang, W.-T. Geng, VASPKIT: A user-friendly interface facilitating high-throughput computing and analysis using VASP code, Comput. Phys. Commun. 267 (2021) 108033.
[51] K. Momma, F. Izumi, VESTA 3 for three-dimensional visualization of crystal, volumetric and morphology data, J. Appl. Crystallogr. 44 (2011) 1272–1276.
[52] S.W. Koh, L. Rekhi, Arramel, M.D. Birowosuto, Q.T. Trinh, J. Ge, W. Yu, A.T. S. Wee, T.S. Choksi, H. Li, Tuning the work function of MXene via surface functionalization, ACS. Appl. Mater. Interfaces. (2023).
[53] M. Zhang, G. Gao, A. Kutana, Y. Wang, X. Zou, J.S. Tse, B.I. Yakobson, H. Li, H. Liu, Y. Ma, Two-dimensional boron–nitrogen–carbon monolayers with tunable direct band gaps, Nanoscale 7 (2015) 12023–12029.
[54] W.G. Hoover, Canonical dynamics: equilibrium phase-space distributions, Phys. Rev. A 31 (1985) 1695–1697.
[55] G. Henkelman, A. Arnaldsson, H. Jónsson, A fast and robust algorithm for Bader decomposition of charge density, Comput. Mater. Sci. 36 (2006) 354–360.
[56] H. Yang, Z. Wang, H. Ye, K. Zhang, X. Chen, G. Zhang, Promoting sensitivity and selectivity of HCHO sensor based on strained InP3 monolayer: A DFT study, Appl. Surf. Sci. 459 (2018) 554–561.
[57] C. Gao, Y. Zhang, H. Yang, Y. Liu, Y. Liu, J. Du, H. Ye, G. Zhang, A DFT study of in doped Tl2O: a superior NO2 gas sensor with selective adsorption and distinct optical response, Appl. Surf. Sci. 494 (2019) 162–169.
[58] S. Sringamprom, T. Thanasarnsurapong, T. Watcharatharapong, W. Hirunpinyopas, W. Sirisaksoontorn, J. Prasongkit, A. Boonchun, Monolayer penta-BeAs2: a promising 2D materials for toxic gas sensor with high selectivity, ACS. Appl. Mater. Interfaces. 16 (2024) 56387–56395.
[59] A. Zhang, H. Yang, Q. Liu, W. Li, Y. Wang, DFT insights into the adsorption properties of toxic gas molecules on pure and transition metal embedded stanene monolayers: Towards gas sensor devices, Synth. Met. 266 (2020) 116441.